

The full-scale avalanche test-site at Lautaret Pass (French Alps)

Emmanuel Thibert, Hervé Bellot, Xavier Ravanat, Frédéric Ousset, Gaëtan Pulfer, Mohamed Naaim, Pascal Hagenmuller, F. Naaim-Bouvet, Thierry Faug, Koichi Nishimura, et al.

▶ **To cite this version:**

Emmanuel Thibert, Hervé Bellot, Xavier Ravanat, Frédéric Ousset, Gaëtan Pulfer, et al.. The full-scale avalanche test-site at Lautaret Pass (French Alps). Cold Regions Science and Technology, 2015, 115, pp.30-41. 10.1016/j.coldregions.2015.03.005 . insu-01164275

HAL Id: insu-01164275
https://insu.hal.science/insu-01164275

Submitted on 16 Jun 2015

HAL is a multi-disciplinary open access archive for the deposit and dissemination of scientific research documents, whether they are published or not. The documents may come from teaching and research institutions in France or abroad, or from public or private research centers.

L'archive ouverte pluridisciplinaire **HAL**, est destinée au dépôt et à la diffusion de documents scientifiques de niveau recherche, publiés ou non, émanant des établissements d'enseignement et de recherche français ou étrangers, des laboratoires publics ou privés.

Cold Regions Science and Technology 115 (2015) 30–41

Contents lists available at ScienceDirect

Cold Regions Science and Technology

journal homepage: www.elsevier.com/locate/coldregions

The full-scale avalanche test-site at Lautaret Pass (French Alps)

Emmanuel Thibert [a,b,*], Hervé Bellot [a,b], Xavier Ravanat [a,b], Frédéric Ousset [a,b], Gaëtan Pulfer [a,b], Mohamed Naaim [a,b], Pascal Hagenmuller [a,b], Florence Naaim-Bouvet [a,b], Thierry Faug [a,b,c], Koichi Nishimura [d], Yoichi Ito [d,a,b], Djebar Baroudi [e], Alexander Prokop [f], Peter Schön [f], Alvaro Soruco [g], Christian Vincent [h,b], Ali Limam [i], Raphaële Héno [j]

[a] IRSTEA, UR ETGR, 2 rue de la Papeterie, 38402 Saint Martin d'Hères Cedex, France
[b] Université Grenoble Alpes, 38041 Grenoble, France
[c] School of Civil Engineering, University of Sydney, NSW 2006, Australia
[d] Nagoya University, Furo-cho, Chikusa-ku, Nagoya 464-8601, Japan
[e] Aalto University School of Engineering, Aalto University, FIN-00076 Aalto, Finland
[f] Institute of Mountain Risk Engineering, 82 Peter Jordan-Straße, 1190 Vienna, Austria
[g] IGEMA-UMSA, Calle 27, Campus Universitario Cota Cota, Casilla 35140, La Paz, Bolivia
[h] LGGE, CNRS-UJF, 54 rue Molière, 38402 Saint Martin d'Hères cedex, France
[i] INSA-Lyon, UR LGCIE, 20 Av. Albert Einstein, 69621 Villeurbanne, France
[j] ENSG, IGN, 6 et 8 Avenue B. Pascal, Cité Descartes, Champs-sur-Marne, 77455 Marne la Vallée Cedex 2, France

ARTICLE INFO

Article history:
Received 5 November 2014
Received in revised form 2 March 2015
Accepted 13 March 2015
Available online 18 March 2015

Keywords:
Avalanche science
Avalanche test-site
Instrumentation
Impact pressure
Avalanche dynamics

ABSTRACT

The full-scale avalanche test site at Lautaret Pass in the southern French Alps has been used by IRSTEA-Cemagref Research Institute since 1972. Over recent years, two avalanche paths have been used routinely to release avalanches and study avalanche dynamics and interactions between avalanches and obstacles. Avalanche flows are generally dense and dry, sometimes with a powder cloud on top. Main avalanche path no. 2 is dedicated to studies on avalanche dynamics. Within the flow of the avalanche, flow height and vertical profiles of pressure and velocity are measured along a 3.5 m tripod. The snow volume released in the release zone is quantified by differential analysis of laser scanning measurements performed before and after triggering. High-speed positioning of the avalanche front along the track is carried out by terrestrial oblique photogrammetry. Above the dense layer, the upper layer of the avalanche is characterized by particle and air flux measurements. Avalanche path no. 1 is smaller in size and particularly well-suited to experiments on structures exposed to small to medium-size avalanches (<1000 m^3). A macroscopic sensor structure consisting of a one square-meter plate supported by a 3.5 m high steel cantilever beam is fixed in the ground, facing the avalanche. Impact pressures are reconstructed from the beam deformations and avalanche velocity is measured by optical sensors. For these experimental devices dedicated to improving our understanding of avalanche physics, a national and international partnership has been developed over the years, including INSA de Lyon, CNRS and Université Joseph Fourier (France), Aalto University (Finland), Nagoya University (Japan), Boku University (Austria) and IGEMA (Bolivia).

© 2015 The Authors. Published by Elsevier B.V. This is an open access article under the CC BY-NC-ND license (http://creativecommons.org/licenses/by-nc-nd/4.0/).

1. Site

The Lautaret full-scale avalanche test site (southern French Alps, 45.033°N/6.404°E) of IRSTEA-Cemagref Research Institute is well-known to avalanche specialists for its long experimental history going back to 1972 (Thibert et al., 2013a; Barbolini and Issler, 2006; Eybert-Berard et al., 1978; Issler, 1999; Naaim et al., 2004). Two avalanche paths (Fig. 1) are located on the southeast slope of Chaillol Mountain (max. 2600 m a.s.l.) near Lautaret Pass (2058 m a.s.l.). On path no. 1, a strong concrete foundation has been built to support equipment for experiments focusing on avalanche interactions with obstacles and impact pressure on structures. Avalanche dynamics are more specifically studied on path no. 2 where a 3.5 m high tripod support is located on the path to measure velocity and pressure within the flow.

On the average, one or two small to medium avalanches have been triggered artificially each winter since 1973, with up to three or four releases in certain winters (see Meunier et al., 2004). Avalanche flows are generally dense and dry, with a small powder cloud on top. The

* Corresponding author at: IRSTEA, UR ETGR, 2 rue de la Papeterie, 38402 Saint Martin d'Hères Cedex, France.
E-mail address: emmanuel.thibert@irstea.fr (E. Thibert).

http://dx.doi.org/10.1016/j.coldregions.2015.03.005
0165-232X/© 2015 The Authors. Published by Elsevier B.V. This is an open access article under the CC BY-NC-ND license (http://creativecommons.org/licenses/by-nc-nd/4.0/).

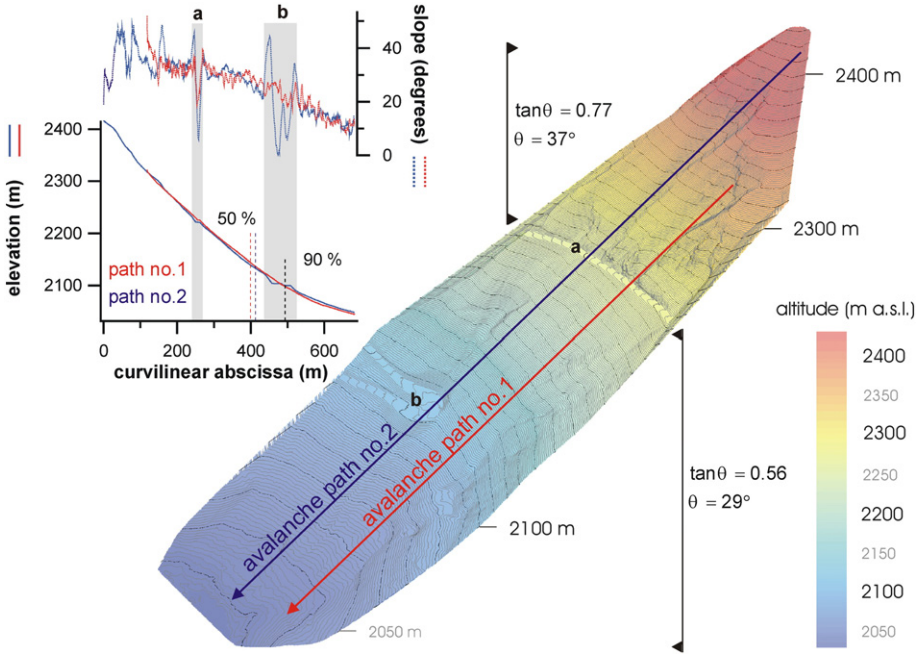


Fig. 1. Topography of the North-East face of Chaillol Mountain used to release avalanches. Major contour lines are at 10-meter intervals. Arrows display avalanche paths no. 1 and no. 2. Letters (a) and (b) refer to locations where avalanche path no. 2 crosses Galibier road. The elevation and slope profiles of both paths are also reported. Average slopes for both avalanche paths are indicated for the starting/accelerating and runout zones, i.e., on either side of the road at (a). Vertical dashed lines are the lowest runout elevations for 50 and 90% of artificially released avalanches, respectively.

dense part is usually less than 1 m thick. Typical release volumes vary from 100 to 10,000 m^3 and maximum front speeds can reach 30–40 m/s (Meunier et al., 2004). Dry snow avalanches released in early winter generally exhibit a density of 80 to 160 kg/m^3 in the starting zone and between 300 and 350 kg/m^3 in the deposition area. The overall track lengths are 600 and 700 m for paths no. 1 and no. 2, respectively. Path no. 2, the longest, extends from 2415 down to 2030 m a.s.l. The average slope angle is 37°, reaching 40° in the starting zones. Below these very steep release zones, the flows are well channeled in steep-sided tracks. Avalanches generally develop their maximal velocity at these locations and this is where the measurement structures have been set up. For both paths, the common runout zone is a large and natural open slope of nearly 29°. From the historical database of almost 50 avalanche release operations, 90% of the avalanches (90th percentile) have a runout distance (projected length) of less than 368 m for path no. 1 and less than 488 m for path no. 2 (Meunier et al., 2004). For both avalanche paths, this corresponds to a runout base elevation of 2100 m a.s.l. (Fig. 1). The 50th percentile is at about 2136 m a.s.l. with runout distances of 280 and 415 m for paths no. 1 and no. 2, respectively.

As opposed to others full-scale avalanche test sites in Europe, such as Vallée de la Sionne operated by SLF in Switzerland (Ammann, 1999; Dufour et al., 2004) and Ryggfonn operated by NGI in Norway (Gauer et al., 2007a; Lied et al., 2004), the runout at Lautaret is a natural open slope. The Ryggfonn runout ends at an artificial dam and that of Vallée de la Sionne ends with an inverse slope. Compared to the recently instrumented Italian test site at Seehore (Maggioni et al., 2013), Lautaret is larger, with runout distances nearly twice as long, representing an intermediate length between Seehore and la Sionne. The morphological characteristics of Lautaret and Seehore are however very similar regarding slope and the regular runout zone. A practical consequence of this small to medium size (a typical volume less than 1000 m^3) is that snow deposited on the instrumented structures by avalanches can be easily cleared off and structures are rapidly operational for the next avalanche release. These conditions make this site of particular interest for experiments involving avalanche impacts on structures as performed on path no. 1 (see Section 4).

2. General equipment and instrumentation

2.1. Shelter and data acquisition

A reinforced-concrete shelter for operators and data acquisition is located between the two main avalanche paths no. 1 and no. 2 (Fig. 2) which are separated by around 60 m. The shelter houses the data acquisition equipment. Acquisition operations must be controlled manually. It is therefore not possible to retrieve measurements form natural avalanches as at Vallée de la Sionne (Ammann, 1999). The acquisition system is based on a PXI platform from National Instrument Corporation. We use a combination of modular SCXI and PXI hardware. A general schematic of the measurement system is presented in Fig. 3. Two types of acquisition cards for analog-to-digital conversion are used: PXI-4472 for the lowest sampling rate (24 bits, 3 kHz) channels (pressure, acceleration, deformation, displacement) and PXI-6250 for the highest sampling rate (12 bits, 60 kHz) channels (velocity). Special signal conditioners are used for strain/bridge based sensors (SCXI-1520) and the piezoelectric accelerometer (SCXI-1530). Power for sensors is both supplied internally by SCXI conditioners and externally by a DC linear regulated power supply. Data acquisition and control is driven from an external PC with dedicated software. Data is stored on solid state drive.

2.2. Release systems and snow characterization

Avalanches are currently released manually on path no. 1 by 2 operators with electrically triggered explosive (Sofranex). On path no. 2, they are released by a Gazex radio remote system. This employs a gas explosive tube using a mixture of propane and industrial oxygen. The exploder is connected to a central gas shelter that is controlled remotely by radio transceivers. Information on the physical properties of the snow involved in the avalanche is obtained from snow-pits dug by

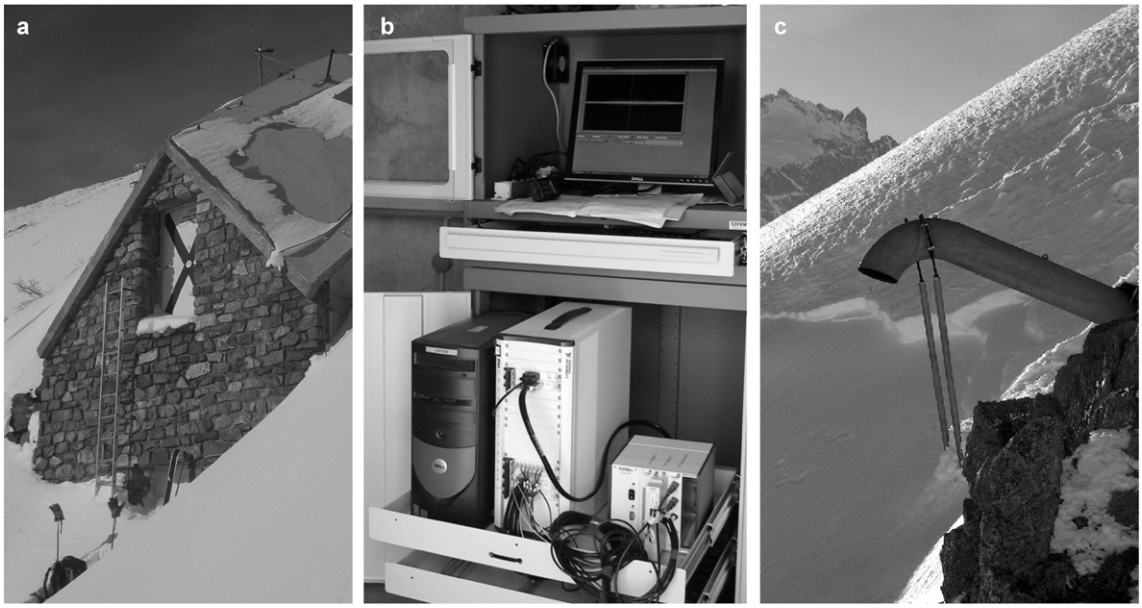


Fig. 2. Shelter housing the operators and the acquisition system (computer, data loggers, power supply): (a) summer view from outside, (b) acquisition system including the PXI and SCXI platform (white chassis) and the external PC. (c) Mouth of the Gazex propane exploder at the top of avalanche path no. 2.

hand close to the release zone. The information includes snow density, temperature, hardness as well as grain types and characteristic size. Atmospheric conditions are monitored by a weather station that records half-hourly averages of air temperature and specific humidity. An overall view of the locations of the measurement and technical infrastructures is mapped in Fig. 4.

3. Instrumentation dedicated to avalanche dynamics

3.1. Pressure and velocity measurements

Avalanche dynamics are specifically studied in the largest avalanche path (path no. 2). A 3.5 m high steel tripod is set up in this path at the end of its steepest part (around 2100 m) where avalanches are expected to reach their maximal velocity (Fig. 5). At this location, pressure and velocity are measured vertically within the flow depth.

3.1.1. Pressure and flow depth measurements

Pressure is measured using full-bridge strain gage based load cells (MGP FM3000). These sensors have been slightly modified from the commercial units to reinforce protection of the wires and control the specially-machined 110 mm diameter circular stainless steel plates used for pressure sensing. The full-scale force measurement range of the strain gages is 50 kN, providing a full-range pressure measurement up to 5260 kPa. The sensors are set up on the uphill-facing side of the tripod and distributed perpendicularly with respect to the main flow each 25 cm (Fig. 5). The dynamic resolution is as low as 0.0013 kPa thanks to the 24 bit digital resolution. The pressure measurement error is estimated at ± 0.47 kPa and is mainly caused by mechanical vibrations of the tripod during the avalanche flow. As a comparison, the typical pressure caused by an avalanche flow is around a few hundred of kPa. Fig. 6 is a typical time plot of the pressure measured along the vertical profile of the flow for an avalanche released in 2009.

To measure the flow height, special pressure sensors are set up on the side of the tripod at 20 cm intervals. They consist of stainless steel plates ($L = 15$ cm long, $e = 1.2$ cm thick and 2 cm wide) equipped with strain gages to measure deformation. Deformation signals are converted into pressure values used to detect if the load is due to the dense part of the flow at the threshold of 3 kPa. The sensors are based on the same principle used for the pressure sensors at Vallée de la Sionne (Baroudi et al., 2011). Here, we use plates of smaller length and width so that the first eigenfrequency is higher (420 compared to 390 Hz at Vallée de la Sionne). The flat frequency response therefore led us to consider a simple static bending mode over the limited 0–100 Hz

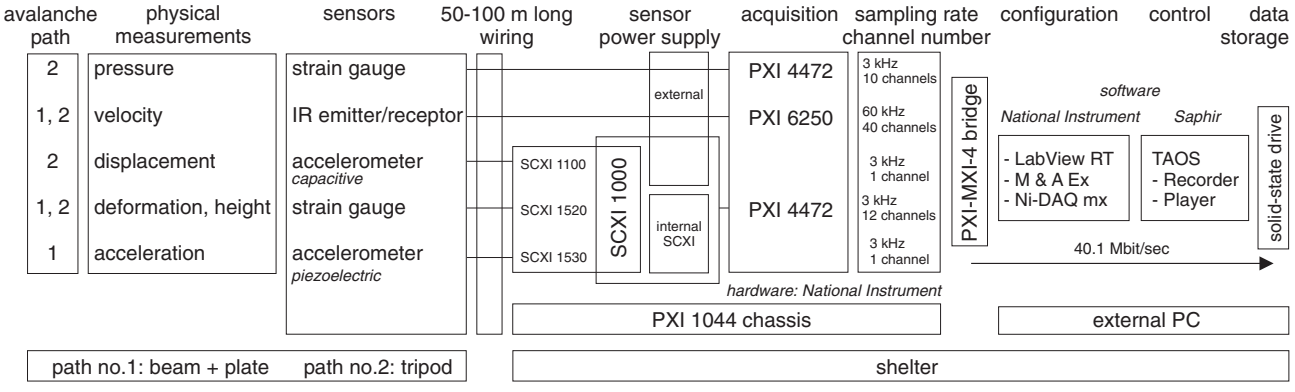


Fig. 3. Schematic of measurements and data acquisition performed within the flow for the 2 avalanche paths, from sensors to data storage. Analog-to-digital conversion is performed by PXI-4472 (24 bits) and PXI-6250 (12 bits) modules. Analog signals conditioned by SCXI modules are multiplexed by the SCXI-1000 platform before digital conversion by the PXI-4472.

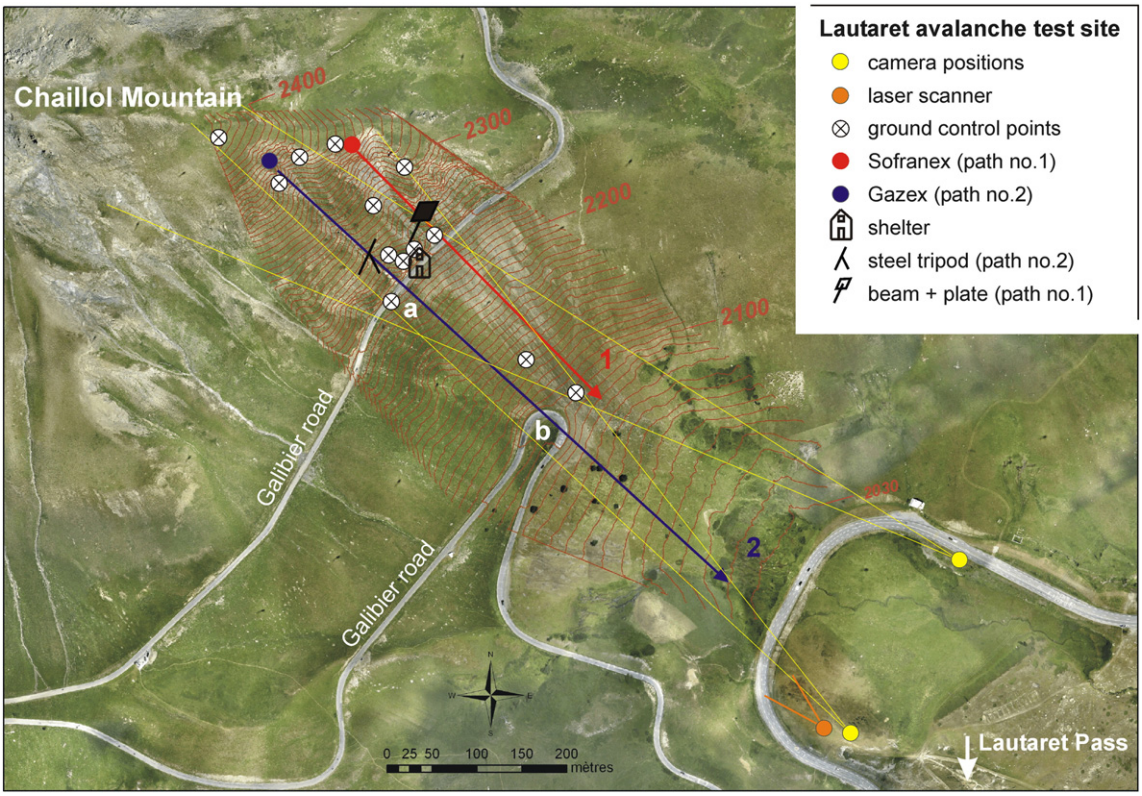


Fig. 4. Aerial orthophotography of the Lautaret avalanche test site. (a) and (b) refer to locations where avalanche tracks cross Galibier road, which is closed in winter (see Figs. 1 and 10). Contour lines are at 5 meter intervals. Yellow lines are the field of view of the stereo cameras.

bandwidth. Higher frequencies are eliminated by a low-pass Butterworth filter. This eliminates the need for the inverse analysis developed for the Valleé de la Sionne sensors to retrieve the pressure signal from the deformation of the plate. The pressure, P, is therefore calculated from the deformation, ε, by the direct relationship (see Berthet-Rambaud et al., 2008; Eq. (4) therein):

$$P = \frac{e^2}{3(L-l)^2} E\varepsilon, \tag{1}$$

where E is the Young's modulus (193 GPa, 304 L grade stainless steel), e and L are the plate width and length, respectively, and l denotes the distance from the embedding location where the deformation is measured by the strain gage.

3.1.2. Velocity measurements

Velocity is measured using the correlation of time-lagged optical signals. This technique was initially developed by Nishimura et al. (1993) and Dent et al. (1998), and is now routinely used at the Vallée De La Sionne (VDLS) avalanche test site (Kern et al., 2009, 2010). These velocity sensors are a typical example of sensors specially developed for avalanche science as no equivalent is available commercially. Their design is based on the assumption that snow grains and grain aggregates do not significantly deform during travel over a distance of a few centimeters. In this case, the optical backscattering of grains and aggregates measured by two infrared sensors at a distance d along the main flow remain correlated with a certain time-lag τ. The velocity v of the passing flow is then estimated as $v = d / \tau$. At Lautaret, we set $d = 0.0076$ m, one-fourth of the flow-wise spacing used at Vallée de la Sionne where larger velocities are observed.

Sensors are mounted in wedge-shaped steel blocks designed to deflect the flow upwards and downwards by a mean angle of 15° (Fig. 5). This ensures proper contact between the flow and the surface of the sensor by avoiding the formation of an air pocket between them. On path no. 1, two sensors are set on the wall-like obstacle pressure sensor and extend outwards into the flow (see Section 4). On path no. 2, velocity sensors are located every 12.5 cm along the tripod to measure the velocity within the depth of the flow (Fig. 5). Our optical velocity sensors were first improved and adapted at laboratory-scale with granular materials and in snow-chutes (Bouchet et al., 2003; Rognon et al., 2008). This represents a significant step forward from the first Lautaret studies in which avalanche velocities were roughly estimated from video recordings at the free-surface of the avalanche flow (e.g., Baroudi and Thibert, 2009).

The time lag τ is determined by analyzing the correlation between the backscattered signals BS_{up} and BS_{do} captured by the uphill and downhill sensors. To compute the time lag $\tau(t)$ at time t, we assume the time lag to be constant over a time frame of width w. Over the interval $[t - w/2; t + w/2]$, the time lag is the value which maximizes the correlation integral CI defined as:

$$CI(t,\tau) = \int_{t-w/2}^{t+w/2} BS_{up}(t) BS_{do}(t+\tau) dt. \tag{2}$$

In practice, we often use a constant width w for an integration interval of about 0.1 s (Fig. 7). Increasing w decreases the velocity time resolution but increases the robustness and accuracy of the method. On the contrary, a smaller value of w makes it possible to capture rapid changes in the velocity, but decreases the robustness of the approach. As shown in Fig. 7, the computed flow velocity is not very sensitive to the adopted w value. It appears also that too short a time integration interval ($w = 0.07$ s) cannot capture the correlation like the 0.1 s time integration interval does at the end of the avalanche ($5\text{ s} < t < 7\text{ s}$). Therefore, the value of w needs to be adjusted depending on the time fluctuations of the velocity signal.

This is done with a series of integrations performed with an incremental dichotomic division of w. This scheme is used to investigate

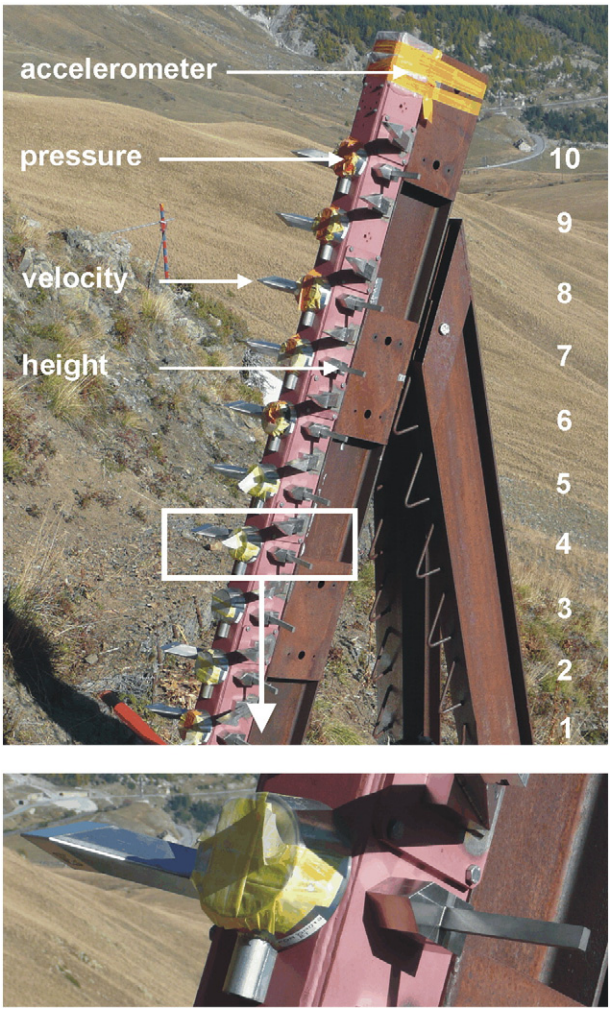


Fig. 5. Top: Steel tripod set up in avalanche path no. 2 and supporting velocity, pressure and height sensors to record the vertical profile within the avalanche. An accelerometer is fixed inside at the top (not visible) to measure the structure displacement for a check on the boundary conditions of the pressure sensors. Numbers refer to pressure measurements plotted in Fig. 6. Bottom: Zoom on the 3 sensors recording at a given flow depth.

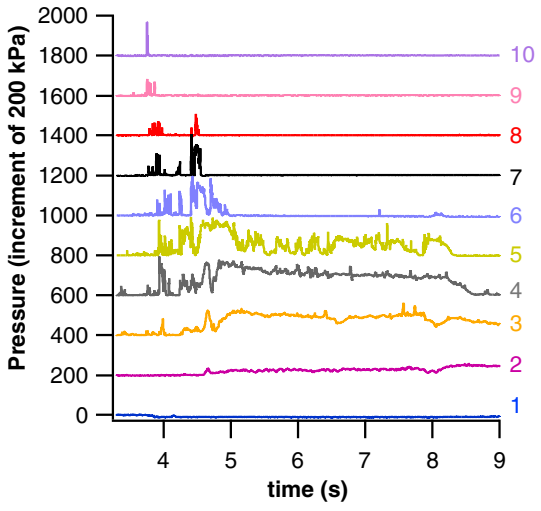


Fig. 6. Vertical pressure profile measured within the flow of the avalanche released on path no. 2 on 9 February 2009. Numbers refer to sensor positions along the tripod as shown in Fig. 5. For legibility, pressure signals are shifted by increments of 200 kPa.

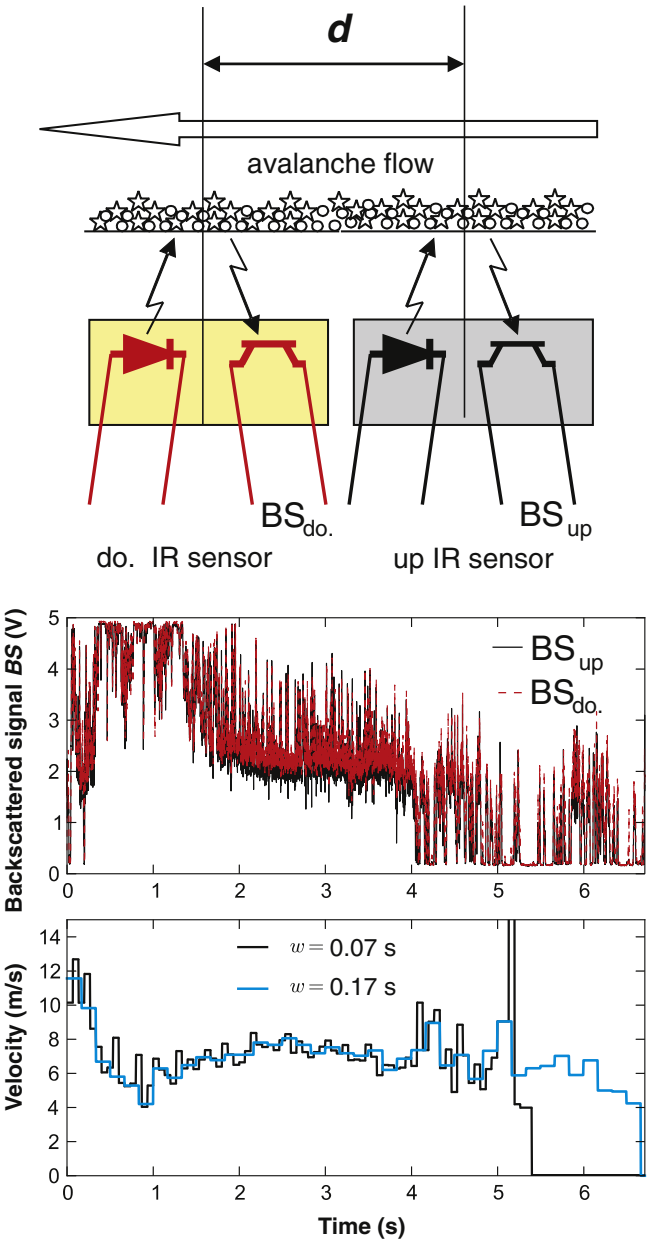


Fig. 7. Measurement velocity within the flow: Top: sketch of the IR sensors backscattering measurement. Middle: example of velocity versus time recorded by the IR sensors for the avalanche released on 18 March 2011 on path no. 1 displaying the backscattered signals from uphill and downhill sensors. Bottom: retrieved velocity with 0.07 and 0.17 s integration time frames for the 18 March 2011 avalanche.

large to small integration time frames and cover long time trends up to high frequency variations of the velocity signal.

3.2. Positioning the avalanche front from photogrammetry

Avalanche fronts on path no. 2 are measured using a high rate photogrammetric system that was developed specifically (Soruco et al., 2011). Positioning avalanches in time can significantly constrain flow simulation from Saint-Venant models, accounting for basal friction along the track and improving our understanding of basal friction processes (Pulfer et al., 2013).

Terrestrial photogrammetry is the only method capable of instantaneously producing a Digital Elevation Model (DEM) during avalanche flow. Alternative techniques, such as laser scanning, require a long

acquisition time that prevents their use to retrieve DEMs during the avalanche flow, although they can be used before and after avalanche triggering to derive snow mass transfer (Bartelt et al., 2012; Maggioni et al., 2013; Prokop, 2008; Sailer et al., 2008). Recent advances in commercially available digital cameras make it possible to acquire up to 4–8 frames per second with high resolution quality. Using numerical reflex Nikon D2Xs cameras (23.7 × 15.7 mm DX format CMOS sensor) with Nikon 85 mm f/1.4 AF fixed focal lenses, the overall avalanche path no. 2 can be measured with one stereoscopic pair of images.

As opposed to Vallet et al. (2001), who used light aerial photogrammetric cameras (Linhof Aerotechnika and Tomtecs HIEI SEII-α) for avalanche mapping at Vallée de la Sionne, and Vallet et al. (2004) who used two professional digital Camcorder (Sony DSR-PD150-P) to track the surface of powder snow avalanches, we used here a low-cost non-metric imagery system. An advanced calibration is therefore required to define a camera model accounting for the radial distortion of the lenses, the decentration of the principal point (principal point shift) and the exact focal length of the lenses for correct scaling of the images (Faig et al., 1990).

Calibration was performed in situ at Lautaret in one operation with an extensive network of 25 ground control points spread over the southeast slope of Chaillol Mountain. Point coordinates were measured using geodetic differential GPS (global positioning system). The camera model and image orientation process were defined using ORIMA software (LeicaGeosystem). Distortion was modeled according to the ISPRS formulation (Gómez-Lahoz et al., 2003) which reads:

$$dr = a_1\left(r^3 - r_0^2 r\right) + a_2\left(r^5 - r_0^4 r\right) + a_3\left(r^7 - r_0^6 r\right), \quad (3)$$

where dr denotes the radial distance between any image point and its ideal radius r, a_1, a_2 and a_3 are polynomial coefficients and r_0 is the radial shift of the principal point which is related to its (x_0, y_0) image Cartesian coordinate system by:

$$r_0 = \sqrt{x_0^2 + y_0^2}. \quad (4)$$

Results of the camera calibration are reported in Table 1 and Fig. 8 plots the radial distortion in the image coordinate system. We found a slight negative barrel distortion reaching 10 μm (1.8 pixel) at corners, which is unusual for long focal length lenses but very low (−0.02% at image corner) considering this non-metric device. For correct scaling of the images, we account for the exact focal length (85.51 mm). The radial shift of the perspective center (80 μm i.e., 15 pixels) is a non-negligible decentration and must also be taken into account in the camera model. This camera model was locked and considered afterward as invariable in the image acquisition, orientation and restitution steps performed for the avalanche experiments.

The photogrammetric method involves 2 mains steps: image orientation and photogrammetric restitution (stereo plotting). They are performed using ARCGIS and ERDAS Stereo Analyst software, respectively. For the triangulation step, we routinely use fewer control points than for calibration, typically between 10 and 16, depending on snow cover conditions. The orientation residual on ground control points in XYZ is around 10 cm, so that a positioning error for resituated points is expected to be less than 25 cm as estimated using the approach presented by

Table 1
Camera model parameters resulting from the calibration.

Camera model parameters	Symbol	Values from calibration
Radial distortion coefficient	a_1	6.24×10^{-6} mm^{-2}
Radial distortion coefficient	a_2	-3.81×10^{-8} mm^{-4}
Radial distortion coefficient	a_3	-4.33×10^{-6} mm^{-11}
Principal point radial shift	r_0	80.03 μm
Principal point coordinates	x_0, y_0	−0.0657 mm, −0.0457 mm
Focal length	f	85.51 mm

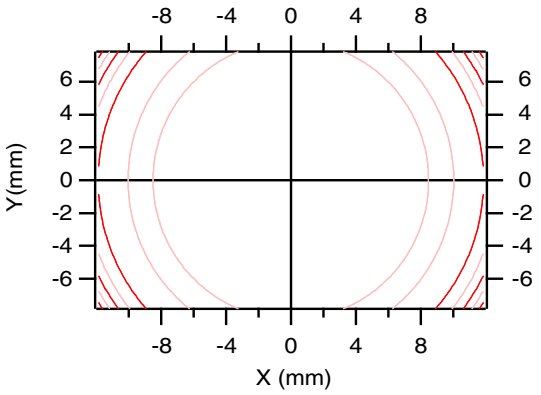


Fig. 8. Radial distortion of the Nikon AF 85 mm f/1.4 AF fixed focal lens. Distortion contour lines are at 2 μm intervals.

Thibert et al. (2008a). The last step of the photogrammetric method is the measurement of three-dimensional coordinates on the photographs. In our case, we perform stereo plotting manually to increase the accuracy because different pixel scales over each photograph due to the oblique sighting tend to corrupt automatic stereo-correlation.

For validation purposes, we compared some photogrammetric measurements on a 100 m^2 surface of a rocky area on the top of path no. 2 to helicopter-borne laser scanning data collected in summer 2006. The number of resituated points was adapted to match the laser scanner point density (10–20/m^2). We obtained very consistent results: no systematic bias is observed in the differences between the surface elevations obtained from the two digital elevation models and the standard deviation is 0.11 m. Fig. 9 displays the obtained digital elevation model differences, showing that the elevation differences are centered and randomly distributed. We also compared the runout position of several avalanches determined with the photogrammetric system to their positions measured with geodetic differential GPS and a total station (tachometer). Measurements were again found to be consistent with discrepancies not exceeding 0.15 m. Both these comparisons provide

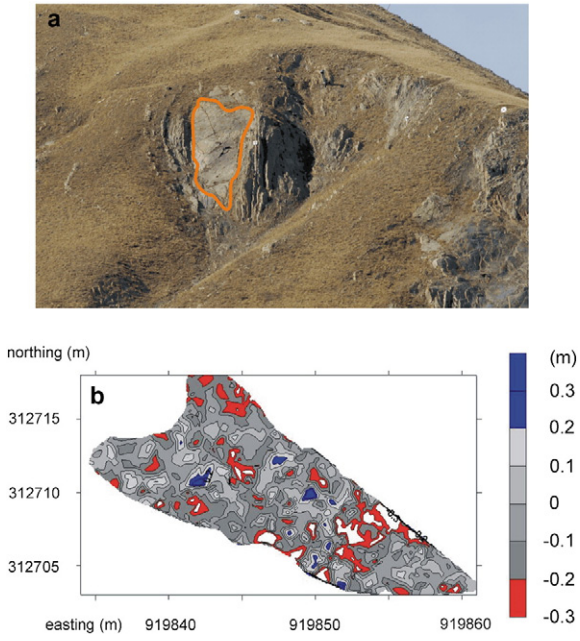


Fig. 9. Comparison between digital elevation models from photogrammetry and laser scanning on a test area. Top: rocky area on the top of path no. 2 use to compare elevation models. Bottom: differences in elevation models: no systematic bias is detected (the average elevation difference is 0) and the standard deviation is 0.11 m.

relative error estimates in the range of 0.10–0.15 m which makes us confident that avalanche front positioning during the flow is accurate.

During avalanche release, the cameras are synchronized with wires to the master clock of a Campbell CR3000 micro-logger. This provides a trigger rate with a precision of 5.7×10^{-6} s. The synchronization error between the cameras has been measured to be around 1–2×10^{-3} s with this triggering system. For an avalanche with a velocity of 10 m/s, we therefore estimate the synchronization to affect the positioning by a few centimeters. Fig. 10 is an illustration of the successive positions of the avalanche released on 13 February 2013 as captured by this photogrammetric method. For the small to medium avalanches often released at Lautaret, the powder cloud is generally limited in size and does not affect the front sighting and plotting on images. Moreover, for safety reasons, we always trigger avalanches under sunny and most of the time clear sky conditions, thereby favoring high contrast on images.

3.3. Powder cloud characterization

New devices have been set up over the last 2 years to investigate the internal structure of the powder part of avalanches released on path no. 2. This research has involved specific collaboration with Nagoya University (Japan). An ultrasonic anemometer (Kaijo TR-61B with a DA-600 signal conditioner) and a Snow Particle Counter (SPC-S7 from Niigata Electric) have been fitted on top of the tripod. The ultrasonic anemometer measures the three-dimensional wind direction and speed in the powder cloud. The wind speed vector is expressed as a down slope component (in the plane parallel to the snow cover at the tripod location) and a vertical component (perpendicular to the slope). The SPC output usually shows the number of particles and particle diameter at each second for mass flux calculation in the blowing snow. However, the diameter and velocity of the snow particles can also be calculated from the high-frequency recorded data of SPC raw signals (60,060 Hz). We routinely consider that the particle concentration in the powder cloud does not affect too much the speed of the sound used to measure the wind velocity from the ultrasonic anemometer. As an illustration, from the measurements performed for the avalanche released on the 10 April 2013, the typical powder density derived from the mass flux and wind speed was about 0.06 kg/m^3. The air density (1.01 kg/m^3 at 2000 m a.s.l. for dry air at 0°C) is therefore increased by 6% due to ice particles. The speed of sound which is proportional to the inverse of the square root of the air density is then just decreased by about 3%. Because the wind speed and particle diameter play a crucial role in powder cloud development, these data reveal the evolution of the powder cloud. Fig. 11 plots the data collected for an avalanche released on 10 April 2013. The first results have been analyzed in Ito et al. (2013).

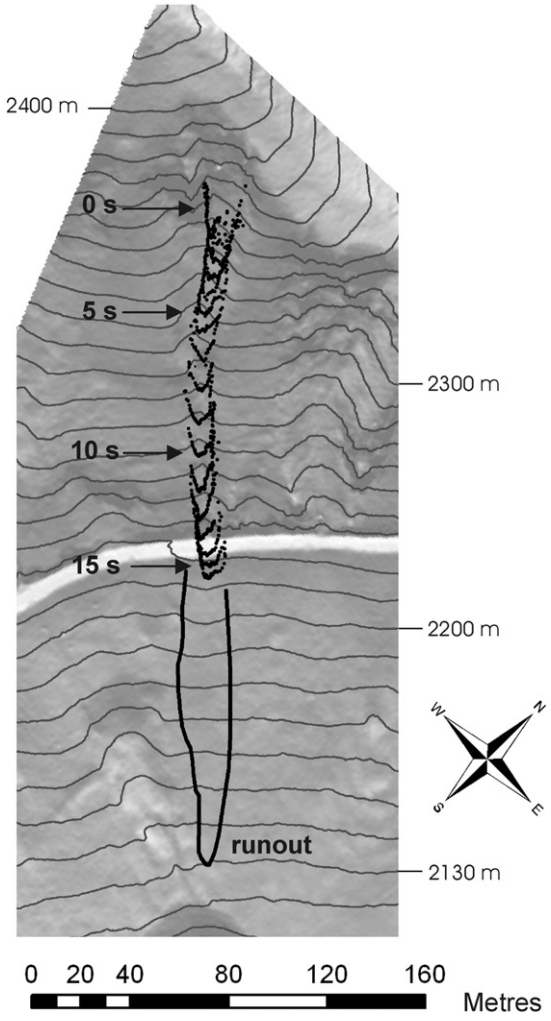


Fig. 10. Successive avalanche front positions as captured by the photogrammetric system on 13 February 2013. The first 16 positions of the front in the upper accelerating part of the avalanche path and the final runout are plotted.

3.4. Initial released volume and mass balance

The released volume sets the initial mass condition for simulating avalanche flow (Sovilla et al., 2007). Another mass input to account for is the entrainment of snow along the track (Eglit and Demidov, 2005; Sovilla and Bartelt, 2002). These mass transfers are quantified from digital elevation models of the snow surface obtained from terrestrial laser scans carried out before and after triggering. This measurement was developed through collaboration with BOKU (Austria). The laser used is the Riegl-321 terrestrial laser scanner operating with a wavelength of 900 nm, which is suitable for snow surfaces (Prokop, 2008). In order to detect changes in the snow surface resulting from the avalanche, two successive scans of the avalanche path are carried out, one prior and

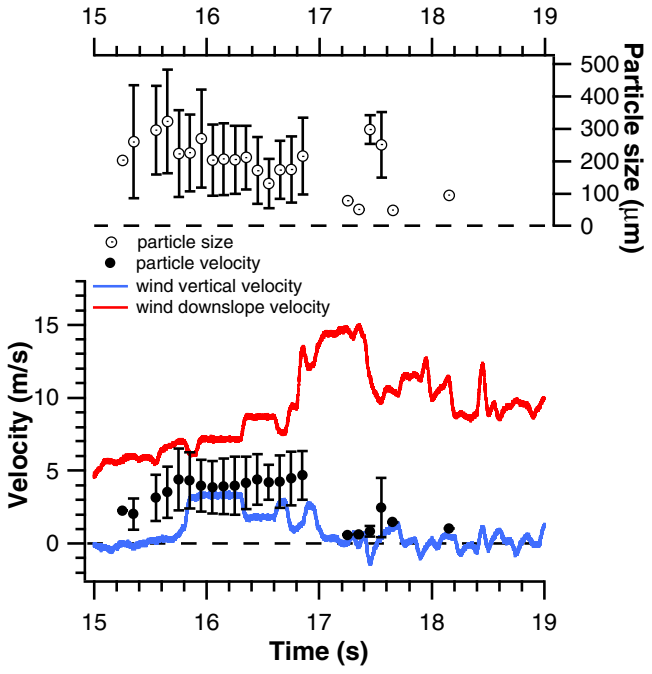


Fig. 11. Powder cloud characterization for the 10 April 2013 avalanche released on path no. 2. Top: Particle size (mean and one standard deviation) measured by the Snow Particle Counter (SPC). Bottom: wind velocity measured with the ultrasonic anemometer and snow particle velocity (mean and one standard deviation) measured with the SPC.

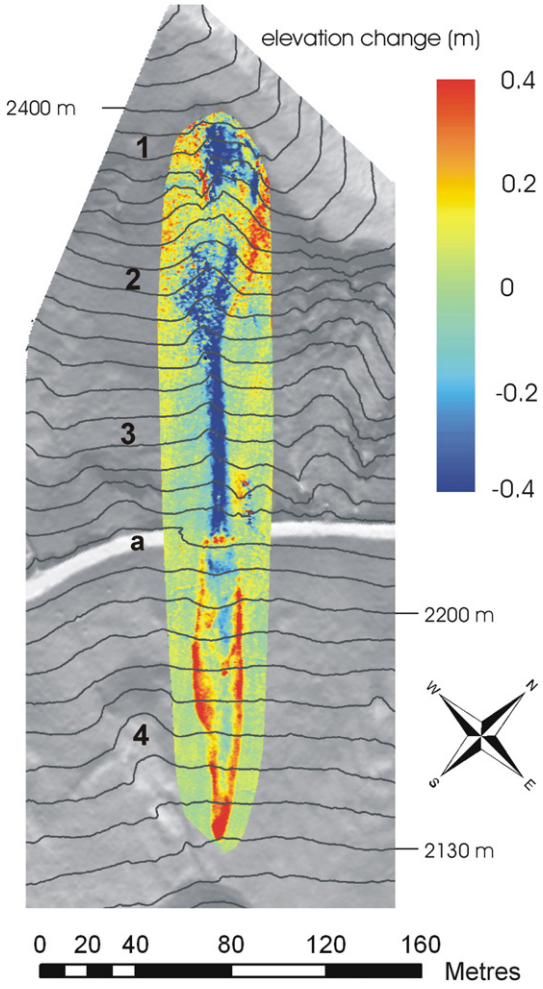


Fig. 12. Map of the elevation difference as measured by laser scanning for the avalanche released on path no. 2 on 13 February 2013. The avalanche path is nearly 380 m long (horizontal distance). The released zone is composed of 2 parts (1) and (2) where the mean released height is 0.12 m. Significant erosion occurs on the avalanche path (3). Deposition occurs from the road at a down to 2130 m (4).

one after the avalanche release. Data is post-processed (co-registration, filtering, and change detection) using the method reported by Prokop and Panholzer (2009). A detailed description of a laser scanning survey is given by Prokop et al. (2015). Fig. 12 shows elevation changes for the avalanche released on path no. 2 on 13 February 2013. This is obtained from the digital elevation model difference and maps the transfer of snow volumes. The release and runout zones are clearly identifiable as well as the erosion process in the upper part of the avalanche track. For the small to medium avalanches often released at Lautaret, entrainment is an important component of mass input.

Regarding error estimates on volumes quantified with the laser scanner, for a single point, the standard deviation in coordinates, σ_{xyz}, is estimated to be within the range of 0.04–0.1 m. An average of $N = 100$ points are generally used to define release areas S within the range of 500–1000 m^2. This results in a volume uncertainty given by:

$$\sigma_{xyz}\, S/\sqrt{N}, \tag{5}$$

i.e., within the range of 10 to 30 m^3. This is an acceptable error as it represents a relative error of around 10% for the smallest released volumes of a few 100 m^3 of snow.

The remote positioning techniques used routinely at Lautaret (photogrammetry, laser scanning) have been validated with direct field total station positioning and geodetic differential global positioning (DGPS). We found very consistent results when plotting the runout of the avalanches from the photogrammetric restitutions, the runout derived from the digital elevation model subtraction obtained from the laser scanner and a direct field survey conducted with DGPS and total station measurements. All measurements were consistent to within ±10–15 cm. An example of comparison between photogrammetry, laser scanning and total station measurements is detailed in Prokop et al. (2015).

4. Impact pressure and flow obstacle interaction

Path no. 1, shorter than path no. 2, generally produces medium-size avalanches, making this track of particular interest for experiments on structures, impact pressure and interaction with the flow (vertical and lateral flow deviation and snow deposits around the obstacle). This research has been carried out for nearly ten years with INSA-Lyon (LGCIE research unit) and Aalto University in Finland (Department of Civil and Structural Engineering), as reported for example by Berthet-Rambaud et al. (2008) as well as Thibert and Baroudi (2010).

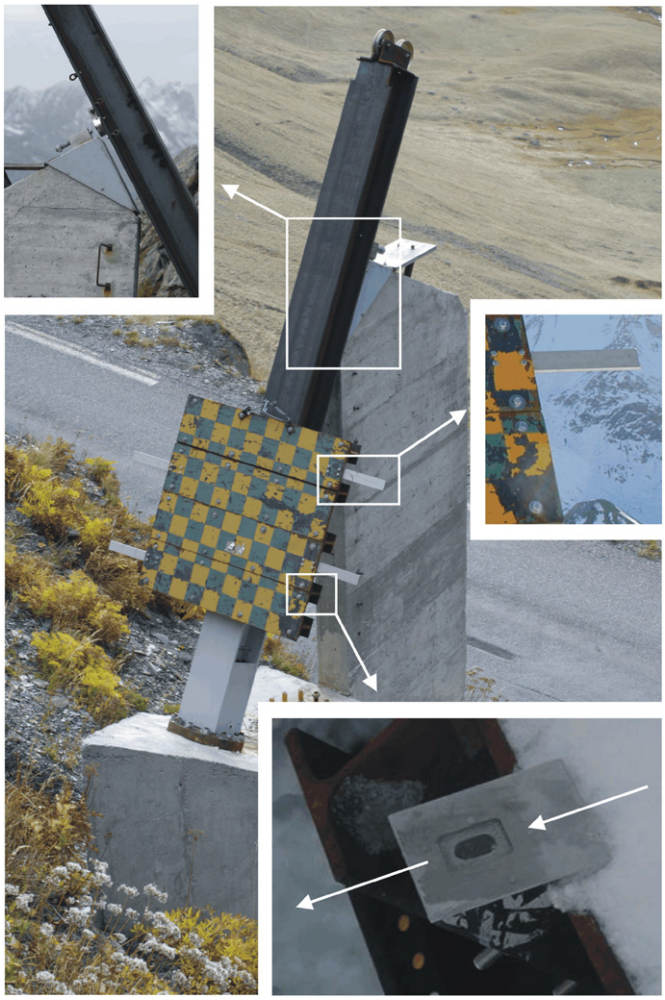


Fig. 13. The instrumented structure set up on path no. 1 including the beam and the 1 m^2 plate system from which loading versus time is used to reconstruct impact pressure from avalanches. The upper inset shows the rear concrete wedge used to avoid plastic deformation of the beam in case if the pressure exceeds 200 kPa. The middle inset shows one of the four cantilever pressure sensors set up on the downhill-facing side of the plate. The bottom inset is a velocity sensor set up on the uphill-facing side of the plate. White arrows show the flow direction on the sensor surface.

4.1. The structure and its deformation

The instrumented structure is a one square-meter plate facing the avalanche, supported by a 3.5 m high steel cantilever beam fixed in a strong concrete foundation (Fig. 13). The plate can be moved along the beam to be located exactly at the surface of the initial snow-cover prior to avalanche release. It represents a large obstacle in comparison to the flow height and therefore integrates the effects of flow heterogeneities. Strains are measured at the bottom of the beam with precision strain gages placed in the maximum bending moment area. The sampling rate for data acquisition is set at 3000 Hz to record dynamic effects. Signals are filtered with a cut-off frequency of 1000 Hz to avoid spectral aliasing.

The structure was designed to deform elastically during avalanche loading. Based on an avalanche sample scenario from Meunier et al. (2004), with a velocity of 30 m/s and a density of 250 kg/m^3, and using a drag coefficient of 2 (Salm et al., 1990), the impact pressure is expected to reach 100 kPa. For standard structural steel (S235, JRG2) with an elastic limit of 235 N/mm^2 and Young's modulus $E = 210$ GPa, and using an HEB beam (HEB-240) with a width of $l = 0.24$ m and a moment of inertia of $I = 1.29 \times 10^{-4}$ m^4, this pressure applied on the 1 m^2 plate set at the maximum height of $L_p = 2.5$ m above the foundation induces a deformation of (Baroudi and Thibert, 2009):

$$\varepsilon = P\frac{L_p l}{2EI}, \tag{6}$$

yielding $\varepsilon = 1.05 \times 10^{-3}$ m/m which is just slightly lower than the elastic limit of 1.12×10^{-3} m/m. To avoid any plastic damage of the beam, its free end is designed to abut a concrete block located 0.019 m behind the beam (Fig. 13).

The expected mechanical deviation, δ, at the free end of the beam can be estimated according to Timoshenko and Young (1956) by:

$$\delta = \frac{1}{3}P\frac{{L_p}^3}{EI}, \tag{7}$$

which gives 1.9 cm at the elastic limit if the plate is located 2.5 m from the top of the beam. The abut force is measured by a 200 kN load cell (Honeywell-Sensotec® type 43) to record the pressure in the event of such overloads.

4.2. Pressure reconstruction

The inverse analysis procedure is developed using dynamic strain measurements performed at the bottom of the structure. The avalanche action is assumed to be uniformly distributed over the plate. No avalanche force is assumed to act directly on the beam which is designed to remain elastic during avalanche loading, perfectly clamped at one end and free elsewhere. The equations of motion are those of structural dynamics (Gerardin and Rixen, 1994) and an Euler–Bernoulli beam model is used.

The direct problem consists in evaluating the strain history from the loading, boundary and initial conditions. Using the Euler–Bernoulli beam model, the direct problem is first solved by assuming that the impacting force acts at a specific point. As described by Meirovitch (1986), this formulation is equivalent to solving a first-order Fredholm integral equation:

$$\varepsilon_i(t) = \sum_j \int_0^t h_{ij}(t-\tau) f_j(\tau) d\tau, \tag{8}$$

where ε_i is the strain history measured at a point x_i (gage locations), f_j the impact load at x_j (center of the plate) and h_{ij} the transfer function between excitation and measurement points. The transfer function or its equivalent Frequency Response Function (FRF) in the frequency domain $\hat{h}(\omega)$, where ω is the angular frequency, is known once the mechanical model of the structure including its boundary conditions has been set (Fig. 14). The FRFs can be also directly measured from impact hammer tests or calculated from numerical finite element computations (Thibert et al., 2008b). As explained in that paper, we use the analytical Euler–Bernoulli beam model, in good agreement with the two other possible FRF calculation methods.

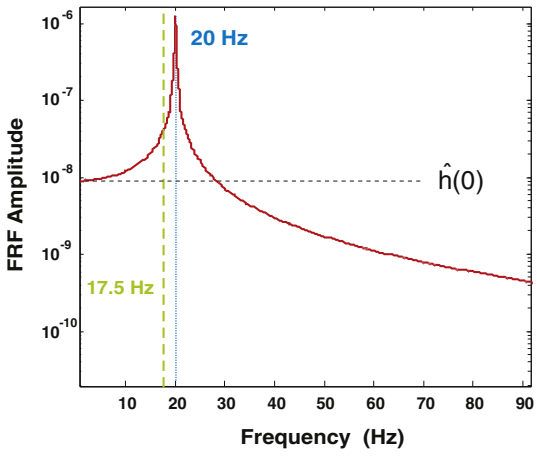


Fig. 14. The Frequency Transfer Function (FRF) deduced from the Euler–Bernoulli direct model of the beam and plate structure. $\hat{h}(0)$ is the FRF at $\omega = 0$ Hz for static loading. The first Eigen mode of the structure (20 Hz) is in the bandwidth of the deformation measurements. The non-linearity of the FRF above 5 Hz (deviation from the constant $\hat{h}(0)$ value) must be accounted for to correctly reconstruct the pressure. The regularization frequency (here 17.5 Hz) shows the final bandwidth available for the reconstructed pressure signal.

The reconstructed avalanche load is obtained from the solution of the inverse problem given by the regularized deconvolution formula:

$$\hat{f}_\delta(\omega) = \frac{\hat{\varepsilon}^\delta(\omega) \cdot \hat{\phi}(\omega)}{\hat{h}(\omega)}, \tag{9}$$

where the symbol "^"denotes Fourier transform functions of the angular frequency variable ω and Φ is the regularization low pass filter. Given that the FRF can have very small amplitudes and that the measured signal $\varepsilon_i(t)$ is polluted by noise, the direct deconvolution of Eq. (9) without regularization ($\Phi = 1$) can render the inverse problem unstable (Tikhonov and Arsenin, 1977). It is therefore necessary to determine the optimal level of regularization, striking a balance between stability and accuracy. This optimal level is achieved using the Morozov discrepancy principle, as explained in our previous studies (Baroudi and Thibert, 2009). From that

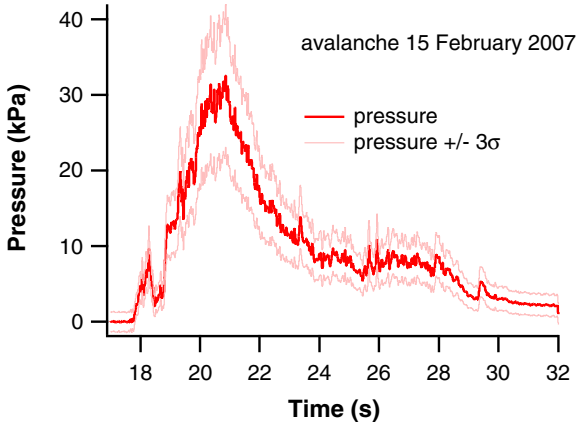


Fig. 15. Reconstructed impact pressure for the avalanche released on 15 February 2007 (from Thibert et al., 2008a,b). The pressure at $\pm 3\sigma$ is estimated from Baroudi and Thibert (2009).

paper, it was estimated that pressure is reconstructed to within a relative error of 10%. Fig. 15 plots a reconstructed pressure signal for an avalanche released on 15 February 2007. In our measurement device is based on a principle close to that more recently developed at the Seehore test-site (Barbero et al., 2013) as it measures the overall pressure on a wall-like obstacle. The technical aspects however differ, as the Italian structure is a multi-element structure with several load cells providing signals that must be summed to get the total pressure.

In order to obtain complementary pressure measurements in avalanche path no. 1 with sensor area comparable to those used in path no. 2, and compare these measurements with the overall pressure obtained by the plate and beam structure-sensor, four cantilever sensors (0.0125 m^2) where set up flush on both sides of the plate and located 0.15, 0.35, 0.60 and 0.85 m vertically above the bottom (Fig. 13). We used strain-gage cantilever sensors derived from those used in Vallée de La Sionne (Baroudi et al., 2011), but smaller in thickness (1 cm against 3 cm) to adjust to the encountered lower loads at Lautaret. Under this geometric condition, the first eigenfrequency of the cantilever is 131 Hz (against 390 Hz at Vallée de la Sionne). Pressure is also reconstructed from an inverse analysis of the recorded deformation, and a regularization frequency in the range of 200–250 Hz is generally used to achieve the Morozov discrepancy principle.

A comparison of these two types of measurements, from small surface sensors and the 1 m^2 plate is plotted in Fig. 16 for the avalanche released on 15 February 2007. The comparison shows that the cantilevers produce higher values in terms of variability and mean values of impact pressure than the 1 m^2 plate. In average, the 4 cantilever signals overpass the plate pressure signal by a ratio within the range of 1.6 to 2.9. This effect has also been reported in an analysis of Sovilla et al. (2014) with an analogous ratio for dry-snow avalanches released at Vallée de la Sionne. This result also confirming the preliminary findings of Baroudi et al. (2011) regarding the effect of the shape and size of the sensor on the impact pressure measured in wet-snow avalanches.

Velocity measurements are also performed on path no. 1 using the same measurement principle as that used for the sensors set up on the tripod on path no. 2. Optical velocity sensors are placed flush on the sides of the plate, extending outwards into the flow. They are located 0.35 and 0.65 m vertically above the bottom of the plate (Fig. 13). Sensors are mounted in wedge-shaped steel blocks designed to deflect the flow upwards and downwards by a mean angle of 15° (Fig. 5). This ensures proper contact between the flow and the surface of the sensor by avoiding the formation of an air pocket between them. Fig. 7 shows the plot of the velocity signals obtained for an avalanche released on 18 March 2011.

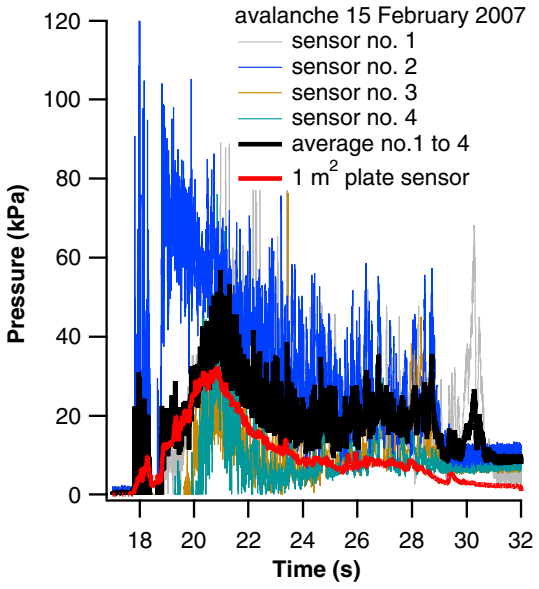


Fig. 16. Comparison of pressure versus time signals recorded by the 1 m^2 plate and the cantilever sensor nos. 1 to 4 (from the bottom to the top of the plate) for the avalanche released on 15 February 2015.

These pressure signals combined with the velocity measurements provide essential full-scale data to estimate the impact pressure of an avalanche on this plate-like obstacle. Effort should be made in the future to set up height sensors in avalanche path no. 1 in the vicinity of the plate-like obstacle. This impact pressure depends on the free pressure of the avalanche flow and on the obstacle drag coefficient. It is a function of the velocity of the avalanches but presents a complex dependence according to the relative contribution of the inertial and gravitational flow regimes (Thibert et al., 2013b; Baroudi and Thibert, 2009; Faug et al., 2010; Gauer et al., 2007a; Naaim et al., 2008; Sovilla et al., 2008a, b, 2010).

5. Intended further developments and conclusions

Over the last 10 years, major efforts have been made to update and develop instrumentation systems at the French full-scale avalanche test site at Lautaret Pass. Thanks to an international partnership, extensive data can be provided today to characterize the dense core and powder cloud flow of artificially released avalanches. They include measurements of velocity within the flow from optical sensors, particle size and velocity in the powder part from an ultrasonic anemometer and a snow particle counter, released, entrained and deposited snow volumes from laser scanning, positions of the avalanche front along the path from high-speed oblique terrestrial photogrammetry and the impact pressures of avalanches on a wall-like obstacle from inverse analysis, as well as the characteristics of the snow involved in the flow.

It is however clear that the experimental site has some specific limitations and, despite consistent developments over recent years, still needs to be improved.

A major intrinsic limitation of the Lautaret avalanche test site is its medium size which makes it impossible to release large avalanches with well-developed powder clouds or aerosol-type avalanches. That is why the IRSTEA-Cemagref Research Institute has preferentially developed small-scale physical simulations to study such avalanches (Beghin and Olagne, 1991; Naaim-Bouvet et al., 2002).

Given the topography of the experimental site as well as the south aspect of the starting zones, release operations are carried out quickly after snow falls to avoid spontaneous triggering or stabilization by snow metamorphism.

A positive consequence of this is that avalanches are likely to involve a recent and rather homogeneous snow layer. This characteristic is effectively generally observed in vertical snow pit profiles obtained in the departure and runout zones from regular measurements of grain types and sizes, temperature profile and density before and after release operations. Our avalanches studied over the last 10 years have mostly been dry and cold snow avalanches, however in the context of climate change, more wet snow avalanches should be investigated. In relation to wet snow rheology, the liquid water content of snow layers at the melting point should be measured.

Taking advantage of homogeneous released snow layers, the snow rheology could be characterized by a field scissometer to investigate the snow shear resistance or a coaxial snow rheometer providing a lateral loading, to determine the cohesion and friction parameters. The obtained rheological parameters should be analyzed in relation to friction parameters obtained from the back analysis of shallow flow simulations.

Regarding avalanche dynamics, continuous Doppler radar performed since the 1980s and later the dual frequency pulsed radar measurements have been used to measure avalanche velocities (Gauer et al., 2007b; Rammer et al., 2007; Salm and Gubler, 1985; Schreiber et al., 2001). The last developments of radar measurements have led to Frequency Modulated Continuous Wave (FMCW) phased array 5.3 GHz radars (Ash et al., 2010, 2011) which have been reported to be very efficient to reveal

internal structures in the avalanche and to track individual fronts and surges down the slope (Vriend et al., 2013). With such a device, the point profile obtained in the middle of the flowing zone of path no. 2 could be enhanced by the spatial distribution of the surface velocity of the whole avalanche.

Regarding erosion processes, laser scanner data are very useful to evaluate the spatial distribution of mass exchange. Buried FCMW radars are known to be very efficient to quantify the dynamics of the erosion process. Laser scanner data provide the erosion extent whereas FMCW radar gives the erosion rate. Moreover, a pair of such sensors could also be used to evaluate the local velocity of the avalanche.

Snow density in the avalanche flow is not measured at Lautaret. It is hoped that the system can be improved to include density measurements within the flow at a point (e.g., on the tripod structure of path no. 2). However, the question will remain as to how snow densification occurs along the path from the starting zone to the runout.

Regarding the overall acquisition system, a valuable improvement would be to make it capable of retrieving measurements from spontaneous avalanches, with automatic activation triggered by seismic sensors.

It is hoped that these quantitative and qualitative observations will improve our understanding of avalanche physics, help validate avalanche simulations and contribute to the refining of avalanche hazard mitigation strategies.

Acknowledgments

The authors are grateful to all those who contribute to avalanche release operations. Since 2005, experiments and instrumentation have been funded by Agence Nationale de la Recherche (ANR, OPALE project), INTERREG-Alcotra (Dynaval and MAP3 projects) and Pôle Alpin Risques Naturels. The photogrammetric work has been sustained through the "Bourse Best" grant awarded to Dr. A. Soruco by the IRD research institute. Thanks are due to the anonymous reviewers who helped to improve the paper. We are grateful to Harvey Harder who revised the English of the manuscript.

References

Ammann, W.J., 1999. A new Swiss test-site for avalanche experiments in the Vallée de la Sionne/Valais. Cold Reg. Sci. Technol. 30, 3–11.

Ash, M., Chetty, K., Brennan, P., McElwaine, J., Keylock, C., 2010. FMCW radar imaging of avalanche-like snow movements. Proceedings of the Radar Conference 2010 IEEE, 10–14 May 2010, Arlington (USA), pp. 102–107. http://dx.doi.org/10.1109/RADAR.2010.5494643.

Ash, M., Brennan, P., Vriend, N., McElwaine, J., Keylock, C., 2011. FMCW phased array radar for automatically triggered measurements of snow avalanches. Proceedings of the 8th European Radar Conference: European Microwave Week 2011, "Wave to the Future", 12-14 October 2011, Manchester, pp. 166–169 United Kingdom.

Barbero, M., Barpi, F., Borri-Brunetto, M., Bovet, E., Chiaia, B., De Biagi, V., Frigo, B., Pallara, O., Maggioni, M., Freppaz, M., Ceaglio, E., Godone, D., Viglietti, D., Zanini, E., 2013. A new experimental snow avalanche test site at Seehore peak in Aosta Valley (NW Italian Alps) — part II: engineering aspects. Cold Reg. Sci. Technol. 86, 14–21.

Barbolini, M., Issler, D. (Eds.), 2006. Avalanche test sites and research equipment in Europe: an updated overview. Final Report Deliverable D8, SATSIE Avalanche Studies and Model Validation in Europe (172 pp.).

Baroudi, D., Thibert, E., 2009. An instrumented structure to measure avalanche impact pressure: error analysis from Monte Carlo simulations. Cold Reg. Sci. Technol. 59, 242–250.

Baroudi, D., Sovilla, B., Thibert, E., 2011. Effect of flow regime and sensor geometry on snow avalanche impact pressure measurements. J. Glaciol. 57 (202), 277–288.

Bartelt, P., Bühler, Y., Buser, O., Christen, M., Meier, L., 2012. Modeling mass-dependent flow regime transitions to predict the stopping and depositional behavior of snow avalanches. J. Geophys. Res. Earth Surf. 117 (1) (Article number F01015).

Beghin, P., Olagne, X., 1991. Experimental and theoretical study of the dynamics of powder snow avalanches. Cold Reg. Sci. Technol. 19, 317–326.

Berthet-Rambaud, P., Baroudi, D., Limam, A., Thibert, E., Taillandier, J.-M., 2008. Characterization of avalanche loading on impacted structures: a new approach based on inverses analysis. J. Glaciol. 54 (185), 324–332.

Bouchet, A., Naaim, M., Ousset, F., Bellot, H., Cauvard, D., 2003. Experimental determination of constitutive equations for dense and dry avalanches: presentation of the set-up and first results. Surv. Geophys. 24, 525–541.

Dent, J.D., Burrell, K.J., Schmidt, D.S., Louge, M.Y., Adams, E., Jazbutis, T.G., 1998. Density, velocity and friction measurements in a dry snow avalanche. Ann. Glaciol. 26, 247–252.

Dufour, F., Ammann, W.J., Bartelt, P., 2004. Swiss dynamic avalanche test site "Vallée de la Sionne". In: Naaim, M., Naaim-Bouvet, F. (Eds.), "Snow and Avalanche Test Sites", Proceedings of the International Seminar on Snow and Avalanche Test Sites, Grenoble (France), 22–23 November 2001. Cemagref Editions, Antony, France, pp. 9–23.

Eglit, M.E., Demidov, K.S., 2005. Mathematical modelling of snow entrainment in avalanche motion. Cold Reg. Sci. Technol. 43, 10–23.

Eybert-Berard, A., Perroud, P., Brugnot, A., Mura, R., Rey, L., 1978. Mesures dynamiques dans l'avalanche — Résultats expérimentaux du Col du Lautaret (1972–1978). Proceedings of the Second International Meeting on Snow and Avalanches, 12–14 April 1978, Grenoble, France, ANENA, Grenoble, France, pp. 203–224.

Faig, W., Shih, T.Y., Liu, X.S., 1990. A non-metric stereo system and its calibration. Proceeding of the ACSM-ASPRS Annual Convention, Denver, Colorado (USA) vol. 5, pp. 18–25.

Faug, T., Chanut, B., Beguin, R., Naaim, M., Thibert, E., Baroudi, D., 2010. A simple analytical model for pressure on obstacles induced by snow avalanches. Ann. Glaciol. 51 (54), 1–8.

Gauer, P., Issler, D., Lied, K., Kristensen, K., Iwe, H., Lied, E., Rammer, L., Schreiber, H., 2007a. On full-scale avalanche measurements at the Ryggfonn test site, Norway. Cold Reg. Sci. Technol. 49, 39–53.

Gauer, P., Kern, M., Kristensen, K., Lied, K., Rammer, L., Schreiber, H., 2007b. On pulsed Doppler radar measurements of avalanches and their implication to avalanche dynamics. Cold Reg. Sci. Technol. 50 (1), 55–71.

Gerardin, M., Rixen, D., 1994. Théorie des vibrations: application à la dynamique des structures. Masson, Paris, France.

Gómez-Lahoz, J., Cuadrado-Méndez, O., Martínez-Rubio, J., 2003. Lens distortion simulation. An application for understanding geometric distortion. Proceeding of the XIXth International CIPA Symposium, 30 September–4 October 2003, Antalya (Turkey), pp. 1–7.

Issler, D., 1999. European avalanche test sites. In: Issler, D. (Ed.), Overview and Analysis in View of Coordinated Experiments. Eidg. Inst. Schnee und Lawinenforsch, Mitt. 59.

Ito, Y., Nishimura, K., Naaim-Bouvet, F., Bellot, H., Ravanat, X., Thibert, E., 2013. Wind and snow particle distribution in powder snow cloud. Proceedings of the International Snow Science Workshop (ISSW'13, October 7-11, 2013, Grenoble- Chamonix Mont Blanc, France), pp. 770–774.

Kern, M.A., Bartelt, P., Sovilla, B., Buser, O., 2009. Measured shear rates in large dry and wet snow avalanches. J. Glaciol. 55 (190), 327–338.

Kern, M.A., Bartelt, P., Sovilla, B., 2010. Velocity profile inversion in dense avalanche flow. Ann. Glaciol. 51 (54), 27–31.

Lied, K., Moe, A., Kristensen, K., Issler, D., 2004. Ryggfonn. Full scale avalanche test site and the effect of the catching dam. In: Naaim, M., Naaim-Bouvet, F. (Eds.), "Snow and Avalanche Test Sites", Proceedings of the International Seminar on Snow and Avalanche Test Sites, Grenoble (France), 22–23 November 2001. Cemagref Editions, Antony, France, pp. 25–98.

Maggioni, M., Freppaz, M., Ceaglio, E., Godone, D., Viglietti, D., Zanini, E., Barbero, M., Barpi, F., Borri-Brunetto, M., Bovet, E., Chiaia, B., De Biagi, V., Frigo, B., Pallara, O., 2013. A new experimental snow avalanche test site at Seehore peak in Aosta Valley (NW Italian Alps) — part I: conception and logistics. Cold Reg. Sci. Technol. 85, 175–182.

Meirovitch, L., 1986. Elements of Vibration Analysis. 2nd edition. McGraw-Hill, New York.

Meunier, M., Ancey, C., Taillandier, J.M., 2004. Fitting avalanche-dynamics models with documented events from the Col du Lautaret site (France) using the conceptual approach. Cold Reg. Sci. Technol. 99, 55–66.

Naaim, M., Taillandier, J.M., Bouchet, A., Ousset, F., Naaim-Bouvet, F., Bellot, H., 2004. French avalanche research: experimental test sites. In: Naaim, M., Naaim-Bouvet, F. (Eds.), "Snow and Avalanche Test Sites", Proceedings of the International Seminar on Snow and Avalanche Test Sites, Grenoble (France), 22–23 November 2001. Cemagref Editions, Antony, France, pp. 141–169.

Naaim, M., Faug, T., Thibert, E., Eckert, N., Chambon, G., Naaim, F., Bellot, H., 2008. Snow avalanches pressure on obstacles. Proceedings of the International Snow Science Workshop 2008, 21–27 September 2008, Whistler, BC, Canada, International Snow Science Workshop Canada Inc. (eds), pp. 740–746.

Naaim-Bouvet, F., Naaim, M., Bacher, M., Heiligenstein, L., 2002. Physical modelling of the interaction between powder avalanches and defence structures. Nat. Hazards Earth Syst. Sci. 2, 193–202.

Nishimura, K., Maeno, N., Sandersen, F., Kristensen, K., Norem, H., Lied, K., 1993. Observations of the dynamic structure of snow avalanches. Ann. Glaciol. 18, 313–316.

Prokop, A., 2008. Assessing the applicability of terrestrial laser scanning for spatial snow depth measurements. Cold Reg. Sci. Technol. 54, 155–163.

Prokop, A., Panholzer, H., 2009. Assessing the capability of terrestrial laser scanning for monitoring slow moving landslides. Nat. Hazards Earth Syst. Sci. 9, 1921–1928.

Prokop, A., Schön, P., Singer, F., Pulfer, G., Naaim, M., Thibert, E., Soruco, A., 2015. Determining avalanche modelling input parameters using terrestrial laser scanning technology. Cold Reg. Sci. Technol. 110, 223–230.

Pulfer, G., Naaim, M., Thibert, E., Soruco, A., 2013. Retrieving avalanche basal friction law from high rate positioning of avalanches. Proceeding of the International Snow Science Workshop (ISSW'13, October 7-11, 2013, Grenoble - Chamonix Mont-Blanc, France), pp. 1418–1424.

Rammer, L., Kern, M., Gruber, U., Tiefenbacher, F., 2007. Comparison of avalanche-velocity measurements by means of pulsed Doppler radar, continuous wave radar and optical methods. Cold Reg. Sci. Technol. 50, 35–54.

Rognon, P.G., Chevoir, F., Bellot, H., Ousset, F., Naaim, M., Coussot, P., 2008. Rheology of dense snow flows: inferences from steady state chute-flow experiments. J. Rheol. 52 (3), 729–748.

Sailer, R., Fellin, W., Fromm, R., Jörg, P., Rammer, L., Sampl, P., Schaffhauser, A., 2008. Snow avalanche mass-balance calculation and simulation-model verification. Ann. Glaciol. 48, 183–192.

Salm, B., Gubler, H., 1985. Measurement and analysis of the motion of dense flow avalanches. Ann. Glaciol. 6, 26–34.

Salm, B., Burkard, A., Gubler, H. U., 1990. Calcul des Avalanches: une méthode pour le praticien avec des exemples. Translated by C. Ancey. Rapport du SLF no. 47, Davos (Switzerland). p. 37.

Schreiber, H., Randeu, W.L., Schaffhauser, H., Rammer, L., 2001. Avalanche dynamics measurement by pulsed Doppler radar. Ann. Glaciol. 32, 275–280.
Soruco, A., Thibert, E., Vincent, C., Blanc, R., Héno, R., 2011. Measurement of avalanche front velocity from high-speed terrestrial digital photogrammetry. Geophys. Res. Abstr. 13, EGU2011–EGU8177.
Sovilla, B., Bartelt, P., 2002. Observations and modelling of snow avalanche entrainment. Nat. Hazards Earth Syst. Sci. 2, 169–179.
Sovilla, B., Margreth, S., Bartel, P., 2007. On snow entrainment in avalanche dynamics calculations. Cold Reg. Sci. Technol. 47, 69–79.
Sovilla, B., Schaer, M., Rammer, L., 2008a. Measurements and analysis of full-scale avalanche impact pressure at Vallée de la Sionne test site. Cold Reg. Sci. Technol. 51, 122–137.
Sovilla, B., Schaer, M., Kern, M., Bartelt, P., 2008b. Impact pressures and flow regimes in dense snow avalanches observed at the Vallée de la Sionne test site. J. Geophys. Res. 113 (1), F01010.
Sovilla, B., McElwaine, J.N., Schaer, M., Vallet, J., 2010. Variation of deposition depth with slope angle in snow avalanches: measurements from Vallée de la Sionne. J. Geophys. Res. 115, F02016.
Sovilla, B., Margreth, S., Schaer, M., Thibert, E., Fischer, J.-T., Baroudi, D., Ancey, C., 2014. Taking into account wet avalanche load for the design of pylon-like structures. Proceedings of the International Snow Science Workshop 2014, 29 September–3 October 2014, Banff (BC), Canada, pp. 727–732.
Thibert, E., Baroudi, D., 2010. Impact energy of an avalanche on a structure. Ann. Glaciol. 51 (54), 19–28.
Thibert, E., Vincent, C., Blanc, R., Eckert, N., 2008a. Glaciological and volumetric mass balance measurements: an error analysis over 51 years, Sarennes Glacier, French Alps. J. Glaciol. 54 (186), 522–532.
Thibert, E., Baroudi, D., Limam, A., Berthet-Rambaud, P., 2008b. Avalanche impact pressure on an instrumented structure. Cold Reg. Sci. Technol. 54, 206–215.
Thibert, E., Bellot, H., Ravanat, X., Ousset, F., Pulfer, G., Naaïm, M., Naaïm-Bouvet, F., Nishimura, K., Ito, Y., Baroudi, D., Prokop, A., Schön, P., Soruco, A., Vincent, C., Limam, A., Pesaresi, D., 2013a. The full-scale avalanche test site, Lautaret, France. Proceeding of the International Snow Science Workshop, pp. 1358–1365 (ISSW'13, October 7-11, 2013, Grenoble - Chamonix Mont-Blanc, France).
Thibert, E., Faug, T., Bellot, H., Baroudi, D., 2013b. Avalanche impact pressure on a plate-like obstacle. Proceeding of the International Snow Science Workshop, pp. 663–667 (ISSW'13, October 7-11, 2013, Grenoble - Chamonix Mont-Blanc, France).
Tikhonov, A.N., Arsenin, V.Y., 1977. Solutions of Ill-posed Problems. Wiley, Chichester (England).
Timoshenko, S.P., Young, D.H., 1956. Engineering Mechanics. 4th ed. McGraw-Hill, New York (USA).
Vallet, J., Gruber, U., Dufour, D., 2001. Photogrammetric avalanche volume measurements at Vallée de la Sionne, Switzerland. Ann. Glaciol. 32, 141–146.
Vallet, J., Turnbull, B., Joly, S., Dufour, F., 2004. Observations on powder snow avalanches using videogrammetry. Cold Reg. Sci. Technol. 39, 153–159.
Vriend, N.M., McElwaine, J.N., Sovilla, B., Keylock, C.J., Ash, M., Brennan, P.V., 2013. High-resolution radar measurements of snow avalanches. Geophys. Res. Lett. 40 (4), 727–731. http://dx.doi.org/10.1002/grl.50134.